Damage Evolution by Acoustic Emission Features using Hilbert Transform in Composite Materials

Mehrdad Nazmdar Shahri*, Jalal Yousefi*, Mehdi Ahmadi Najfabadi[*1], Mohamad Fotouhi[*]

* Non-destructive Testing Lab, Department of Mechanical Engineering, Amirkabir University of Technology, 424 Hafez Ave, 15914, Tehran, Iran

Abstract

One of the intricate issues of using acoustic emissions (AEs) for mechanical diagnostics in composite materials is establishing a relation between acoustic features and fracture behaviors. Therefore Hilbert Transform (HT) which is a new method to investigate fracture and damage evolution were used to analyze AE features of cross ply polymer composite material subjected to ENF test which simulate mode II delamination. Two different mid-plane interface layups are used. HT is used to extract frequency range of each damages occurring in different stages of loading process for each layup. Phase angle of HT is used as a novel feature to distinguish frequency ranges of AE waveforms and the resulting ranges are correlated to the damage mechanisms of the material under investigation. Three important stages in mode II delamination, i.e. initiation, maximum load nearby and the region where crack reaches to the middle of the specimens, are investigated using the introduced method and the details of damages in those regions are characterized. The results of Hilbert transform was in good agreement with scanning electron microscope (SEM) pictures. As a result, it is shown that AE method accompanied with the presented method is a new appropriate approach to examine damage mechanisms in composite materials.

Keywords: Acoustic Emission, Hilbert Transform, Composite Material, Phase Angle, Delamination

[1] Corresponding author; Tel: (+98 21) 6454 3431; Fax: +98 21 8871 2838; Email address: ahmadin@aut.ac.ir

1. Introduction

Over recent decades, composite structures are extensively used in many applications such as aircraft structure, marine containers, vehicle manufacturing and so on. This is because of their light weight and high strength. For examining these materials, due to their complexity, one of the trustworthy approaches is nondestructive assessment methods for inspection and labelling of these materials. So acoustic emission (AE) as a nondestructive methodology is a suitable instrument to investigate composite materials dynamically. An important issue in AE approach is to identify damage mechanisms using AE signals. Many researchers have employed AE features such as amplitude, Energy and frequency of the signals to determine damage evolution [1-3]. A complete overview of damage recognition using AE is provided in ref [4], in most cases a complementary method is needed for distinguishing damage progression [5-7]. In some studies, unsupervised pattern recognition has implemented to cluster distinct type of damages [8-10]. Huguet et al. [11] characterized AE signals using this technique with neural network linked with K-means algorithm. Tensile test have been applied on unidirectional and cross-ply composite materials in this work. They realized an excessive signature allocating to delamination. However, descriptor-based AE approaches often focus on time features. The key lack of these techniques is that they are not entirely pertinent for characterization of intricate composite materials. So, frequency domain is implemented to categorize failure mechanism [12, 13]. The short time Fourier transform was first utilized for time-frequency determination [14]. In that research, the frequency range of each failure behavior was acquired in composites during tensile test. Some studies have employed wavelet transform examination in order to recognize unique failure mechanisms [15, 16]. Qi et al. [15] implemented discrete wavelet to examine AE records of static loading using unidirectional and cross-ply composites. By the use of energy content of AE signal in each level of decomposition, they obtained the frequency band of each separate damage behaviors. Another relevant technique of damage analyzing for non-stationary signals which has newly been applied is Hilbert Huang transform (HHT). As an example, Peng et al [17] handled Hilbert Huang transform to acquire appropriate descriptor for investigation and feature extraction of vibration signals. Hamdi et al [18] explored composite failure mechanisms in unidirectional glass-fiber reinforced polymer using HHT. They revealed that HHT is an effective tool for damages categorization using AE features of distinct failure. In conclusion, signal processing techniques such as time-scale or time-frequency analysis of AE waveforms are reliable methods to obtain damage mechanisms.

In this paper, Hilbert Transform was used to extract frequency feature of each AE signal. The innovation of this approach is to discriminate AE signals using instantaneous frequency of each AE waveform. It is shown that the extracted frequency range from HT characterize a distinct type of damage. Then scanning electron microscope (SEM) images were applied to investigate the accuracy of the applied method. After that, the damage mechanisms are discussed in more details in three stages. Finally, the agreement of the discussed method with other researches is obtained.

2. Experimental Procedures

2.1. Description of the Materials

Glass fiber/epoxy materials were used for the experimental work. Rectangular plates of composite plates were manufactured in the lab. It is shown that two main specimen types were used as listed in Table 1.

Table 1 Number of specimens with their stacking sequences

A hand-layup method was employed to manufacture the specimens, after that, a 12 hour vacuum bagged procedure was implemented. A 20 μm Teflon film was used to create a starter crack at mid-plane during molding. The next step was to place the models in open air 48 hour at 20^{o}c. The quality of the plates was checked by the use of ultrasonic c-scan method. In the final step, specimens were acquired by the use of precision band saw. The specimen dimensions were 110*20 mm with thickness of 10 mm.

2.2. Test Method

The ENF (end notch flexure) shown in Fig. 1 consists of a rectangular, uniform thickness, cross ply laminated composite specimens, containing a crack at one end which serves as a delamination initiator. Three points bending was applied with the force at mid-length of the composite beam. In the figure h, L, B and a_0, the dimensions of the samples, are 5, 55, 20 and 40 mm respectively. Two AE sensors were used, one of them was placed at the tip of the crack and the other was located within 10 mm distance.

Fig. 1 The specimen for three points bending test, end notch flexure (ENF)

The 5mm/min rate of loading during all tests was applied using a tensile test machine under constant displacement rate (0.5 to 500 mm/min). Moreover, the AE sensor was a single-crystal piezoelectric transducer with a resonance frequency of 513.28 KHz and an optimum operating range of 100–750 kHz, which was adjusted to 1 MHz. Besides, a data acquisition system with the maximum sampling rate of 40 MHz was used to record AE signals. A pre-amplifier with a gain selector of 40 dB was executed to enhance the receiving signals and the threshold was adjusted to 35 dB. Before each test, pencil lead break method was used to calibrate the AE sensors. Finally, the AE signals were captured during three points bending test.

3. Used Method

3.1. Hilbert Transform

Hilbert transform (HT) is used to choose a companion function y (t) for a real function x (t). Hilbert transform includes some basic steps in signal processing. In the first step, the Fourier transform of the given signal is calculated. After that, the negative frequencies are rejected. As a final point, the inverse Fourier transform is computed. The output is a complex-valued signal which creates real and imaginary parts of Hilbert transform [19]. Hilbert transform can be a useful method to detect a signal features. Many researchers have applied HT in diverse application such as neuro-physiological and auditory prostheses signals analysis [20-22].
The Hilbert transform can be defined as Eq1 and Eq2 [19]:

$$y(t) = H\big(x(t)\big) = \frac{1}{\pi} p \int_{-\infty}^{\infty} \frac{X(\eta)}{t-\eta} d\eta \qquad \text{(Eq1)}$$

$$x(t) = H^{-1}\big(y(t)\big) = -\frac{1}{\pi} p \int_{-\infty}^{\infty} \frac{y(\eta)}{t-\eta} d\eta \qquad \text{(Eq2)}$$

Where p is the Cauchy principal value. So an analytic signal like z (t) can be expressed as following (Eq3):

$$z(t) = x(t) + iy(t) = a(t)e^{i\theta(t)} \qquad \text{(Eq3)}$$

Where

$$a(t) = \big(x^2(t) + y^2(t)\big)^{\frac{1}{2}} \text{And} \theta(t) = arctan\frac{y(t)}{x(t)} \qquad \text{(Eq4)}$$

The above-mentioned $a(t)$ and $\theta(t)$ are respectively instantaneous amplitude and phase angel of $x(t)$.

4. Results and Discussions

4.1. Procedure of damage evolution

The main objective of this work is to investigate AE waveform to establish an appropriate relationship between AE features and damage mechanisms. HT which is a new approach is implemented to extract the frequency content of the AE waveforms for a distinct failure occurring in the composite specimens. In this study, a vast number of separate burst waves were logged during the loading of test samples. Variations in AE events are due to diverse failure mechanisms during the experiment. The waves exceeding the threshold were captured for one micro second. These waves are originated from diverse damage behaviors during the experimental procedure. There are also some waveforms which are not related to damage mechanisms and may be occurred as a result of elastic deformations and etc. For achieving exact information about AE features of damage mechanisms, de-noising the waveforms which are not related to crack initiation and propagation and have amplitude higher than threshold value, is required. Generally, low frequencies are related to secondary mechanical oscillation of the instance, but this fluctuation has rapid peaks and usually damps rapidly. So frequency filters are not useful in detection of such phenomena. In this case the instantaneous frequency concept can

be valuable. For this purpose, the instantaneous frequency of each wave is computed and then the mean value in range of wave length is computed. After that 40 percent of waves with the least mean frequency are eliminated. As it is shown in Fig2, the crack initiation and propagation is detected by this approach.as illustrated in Fig. 2, at the beginning of the loading, small amount of waves passed the threshold and de-noise process, therefore few signals were recorded. As testing time passed, more and more waves were recorded and at the maximum load, the rate of recorded waves reached its peak.

Fig. 2 Force and average number of counts vs. deflection diagram

The main requirement to study the behavior of the damage mechanisms in composite material is to gather the information related to crack initiation and propagation. As it can be seen from figure 3, by considering the cumulative count trends, three different stages for mode II delamination phenomenon are recognized which are as follow:

1) Initiation stage: at this stage delamination starts to propagate. The energy needed for this stage is called critical strain energy. If stored strain energy reaches the critical strain energy delamination damage initiates. In first period, the plot is linear and all the deformations are elastic, the crack is stable in this stage.
2) Sudden propagation of delamination near the max load: The crack initiation and propagation would commence in this stage. Crack propagation is rapid at first, but as it reaches mid- length of the specimen, rate of propagation would diminish. The effect of two opposite variable, one is crack propagation (slope reduction of force augmentation) and the other is rate reduction of crack propagation growth would cause the maximum in the figure. These results are in a good agreement with other researches [23]. Benzeggagh and Kenane [23] have showed that a crucial drop in the load diagram immediately after the point of damage initiation is a characteristic of the propagation instability in pure mode II.

3) Arrest of delamination propagation when crack reaches to the middle of the specimens: In the last phase of this section crack reaches the center of the specimen. In this stage, the rupture of the specimen would start from the center, as it is obvious, the rate of acoustic events would increase and finally the specimen would split from this point.

Fig.3 Cumulative counts of AE events and force (KN) vs. time (second)

Since these three stages are important stages in the case of mode II delamination, therefore by gathering AE information at these stages and applying HT, fracture behaviors of these stages could be signified using AE features.

In addition to create AE reference pattern for this analysis, classification of pure matrix cracking and fiber failures was done by applying pure tensile tests on resin and fiber bundle (see Fig 4).

Fig. 4 Experimental procedure of pure matrix cracking and fiber breakage

According to our previous investigation [24-25], the frequency characteristics of fiber-matrix debonding are considered between matrix cracking and fiber breakage. The results of pure failures are shown in Figs 5, 6 and Table 2.

Fig. 5 Phase angle and Hilbert transform of pure matrix cracking

Fig. 6 Phase angle and Hilbert transform of pure fiber breakage

Table 2 Dominant Frequency (kHz) range of pure failures

Fig.3 Cumulative counts of AE events and force (KN) vs. time (second)

Variation of cumulative AE counts, which causes different above-mentioned stages, is related to different type of damage mechanisms occurred in these stages. Characterization of these damage mechanisms is useful for better understanding of delamination behavior, especially in initiation stages. Therefore the analysis of AE waveforms, corresponding to these stages, was done by applying HT.

4.2. HT results

A main feature which separates this work from other similar researches focusing on various features of extracted waves of AE signals e.g. rise time, count and etc., is the use of instantaneous frequency to separate distinct type of damages. Also this study is focused on characterization of damage mechanisms occurred at diverse stages of mode II delamination. In the used approach, results are obtained from AE signal analysis using HT. The output is an analytical signal, which the real part is input signal and the imaginary section is the Hilbert transform of input signal, and the magnitude is envelope of the input signal. The envelope of the output signal can be defined as equation 4.

The Discrete Hilbert Transform (DHT) is applied using Parks-McClellan technique with 32 filter points. This approach is one of the well-known methods to detect envelope of a diagram. The analytical signal is obtained from multiplying the output of HT by $\sqrt{-1}$ and then adding to delay

of the input signal. The delay is because of inherent delay in computing HT and the real part of the signal should be delayed not to distract two signals occurring simultaneously. The magnitude of the analytical signal is the envelope of the input signal. The frequency content of the envelope is lower than the curve. A filter is used to exclude the high frequency noises in the envelope, which is occurred as a result of using numerical approach.

As it is shown in Fig7, envelope of the curve reaches its maximum magnitude in a short time and after that reaches zero in an exponential trend. It should be considered that this is a regular signal and some signals exist that do not obey this rule, for example they may encounter abrupt changes, but it could be expected that many signals have the same trend in envelope curve according to Fig. 7. In this case by computing Fourier Transform of the main wave, the few parts of the wave having high amplitude, have very fundamental effect on this computation. The main idea of this part is to leave out the exponential reduction of the curve and to reach this goal, the first step is to divide the wave to its envelope and after that the frequency spectra computation is applied.

Fig. 7 A typical sample of acoustic wave with its Envelope trend

In Fig. 8, a signal with high noises is chosen to show usefulness of the applied approach in comparisons to others methods. Otherwise the signal is not completely reversed and symmetric, due to high noises, but the envelope is fully detected. There are some small vibrations in the vicinity of zero amplitude in envelope curve. The reason is that the envelope is directly obtained from Hilbert Transform of the main signal and is not filtered.

Fig. 8 A sample AE wave in three points bending test with its envelope (time(S) vs. amplitude (mV))

As it is shown in Fig. 9, angle phase and envelope are plotted simultaneously. One of the main outcomes of this plot is that when the value of signal reaches zero, amplitude of the envelope identically takes zero value. According to mathematical definition of phase angle, it can choose any value in consecutive zero amplitudes. The Hilbert transform keep the phase angle constant and this is very cooperative in this application. In phase angle diagram, the phase changes (slope of phase angle vs. time) is almost constant and when the plot picks the zero value (AE sensors catch no sound) the value of phase angle remains stable. The slope of aforementioned plot is the mean frequency content which uses as an alternative and effective tool in comparison with conventional methods. Briefly, the procedure of this approach is to determine slope of best fitting of phase angle plot after acquiring HT and define this value as mean frequency.

Fig. 9 approximation of envelope and phase angle vs. time(s)

The slope of phase angle diagram is zero or has the mean frequency value (this is definition and one should find the best fit). For this purpose, firstly, the phase angle-time plot (Fig 10) is passed through low-pass filtering to omit the miniature noises. Then the slope of this plot is computed and its distribution is investigated.

Fig. 10 instantaneous frequency and phase angle vs. time

Fig. 11 is histogram diagram of instantaneous frequency which is extracted from Hilbert Transform. The frequency content of short Fourier transform is plotted in Fig.12. Both of these plots have the peak amplitude of 150 KHz. But the usage of Hilbert transform has some advantages. Firstly, The Hilbert transform extracted the envelope of the curve and this leads to redefine the acoustical parameter. Moreover, the instantaneous frequency shows the frequency content of the wave in every moment. For instance, the root mean square of wave samples is redefined as root mean square of envelope curve. In this work, a technique for crack initiation and propagation detection using area under envelope curve (or coefficient of mean envelope) is elaborated.

Fig. 11 distribution of instantaneous frequency in 2 KHz frequency intervals

Fig. 12 Fourier transform of the main wave

Micrographs of the fracture surfaces were captured using a scanning electron microscope (SEM). Fig. 13 is showed SEM images along the crack of specimens. In ref. [26], it is stated that micro cracks occurring in deformation zone ahead of crack tip are key reason of hackle mark features (shown in Fig.13) due to high energy absorbing mechanism and the more hackle width, the more surface energy dissipation [27].Other observed types of damage is broken pieces of fiber due to micro buckling [28]. For the used cross-ply samples interfaces matrix cracking and debonding fiber/ matrix and rarely fiber breakage was distinguished. Matrix cracking and debonding could discriminate using visco-elastic relaxation procedure in the vicinity of source [29]. The relaxation times τ_i, elastic module E_i and densities ρ_i correlation can apply to distinguish distinct feature of relaxation procedure in the fiber, matrix and matrix/fiber interface according to [29]:

$$f_i \sim 1/c_i \sim \sqrt{\frac{Ei}{\rho i}} \qquad (6)$$

It can be concluded that the epoxy-matrix cracking produce lower wide-band frequencies than the glass-fiber/matrix interface debonding. In conclusion, the connection between prevailing component frequency and failure mode, microscopic observation was applied.

From the above discussion and applying the Hilbert transform to the AE waves at the introduced regions following results about the damage mechanisms of those regions are obtained:
Stage 1) initiation: As indicated in the figure 13 the results of the applied procedures show that at initiation stage, almost all damage mechanisms are related to matrix cracking, it means that delamination in all the cases almost initiates from the matrix which is softer than fibers.
Stage 2) Hilbert function analysis in this region indicates a mixture of different damage mechanisms. As shown in figure 13 combination of matrix cracking, fiber/matrix debonding and fiber breakage are the source of AE waveforms in this region but the percentage of these damages are different and fiber breakage event has small amount of events compared to the other damage mechanisms. Since there is an unstable crack behavior in mode II delamination therefore strong AE signals are appeared at this region. In this step, the crack initiate and due to stress concentration fiber/ matrix debonding is occurred.
Stage 3) at this region the crack reaches the middle of the specimen and the applied load prohibits crack growth. In this region fracture mechanisms are found to be matrix cracking and fiber/matrix debonding and fiber breakage. In this step the growth rate of debonding is higher than fiber breakage and the growth rate of matrix cracking is decreased.

Fig. 13 SEM observation of different failure mechanisms during mode II delamination

It is concluded that components with a phase angle with low frequency (100-190 kHz) is associated with matrix cracking. Another dominant phase angles can directly correspond to other damage mechanisms e.g. debonding between matrix and fiber where the frequency range is 250–310 kHz (extracted from Phase angle analysis). Signals with high frequency (375– 440 kHz) represent fiber breakage failure. The above argument is consistent with the existing research results based on the AE frequency contents of signals [30–32]. In addition, the SEM observation is in agreement with the results obtained from Hilbert transform analysis. Consequently, the other phase angles in HT analysis can be considered as a noise, fiber pull-out and sliding of fibers. In Fig 14, the distribution of the frequency of counts for the above-mentioned three stages is showed. Time periods of the stages are based on reception of AE signals; it means that the length of the periods is based on number of AE events passing the thresholds. The first step is 5 second after crack initiation. In this stage, the dominant mode of failure is matrix cracking. Debonding is another failure which is occurred during this stage but as it is shown in Fig 14, this phenomenon is happened fewer in comparisons with matrix cracking. Fiber breakage is rarely occurred in this stage. Two second after maximum load is considered as the second stage. Three different types of failure are obvious in this stage. The dominant failures are still matrix cracking

and debonding. In the last stage, the rate of matrix cracking occurrence is diminished; the debonding failure is increased due to incidence of matrix cracking in previous stages; Fiber breakage is rarely occurred in comparisons to two other types of damage. The required energy for crack initiation is higher in 0/0 stacking sequence in comparisons to 0/90 layup. The fiber breakage has happened more in 0/0 layup; this is due to more fiber bridging and more fiber volume in direction of loading in 0/0 layup. The more fiber breakage is occurred in maximum load stage in 0/0 layup because of larger fiber length.

Fig. 14 Distribution of Frequency of Counts among all AE waveforms for a Sample Specimen

5. Conclusions

In this study, a new and applicable procedure for investigation of AE signals of distinct failure was proposed. The used method in this case was Hilbert transform. This method has provided a new frequency descriptor for different damages for non-stationary AE signals. By the use of the SEM image, diverse damage mechanisms were distinguished in three points bending test. The correlation between dominant damage mechanisms was established using SEM observations and Hilbert transform. The results showed that HT could be effective technique to evaluate damage mechanisms, and good agreement was established between theoretical and experimental data. The results obtained are interesting since the new approach using phase angle, characterize very well each kind of damage mechanisms. In this case, it is feasible to recognize diffuse damages and to use for in situ health monitoring applications.

References

1. D.J. Yoon, W. Weiss and S.P. Shah, Assessing damage corroded reinforced concrete using in acoustic emission, Journal of Engineering Mechanics., 2000, pp. 273–283.
2. A.G. Magalhaes and M.F. de Moura, Application of acoustic emission to study creep behavior of composite bonded lap shear joints, NDT&E International, 2005, 38 :45–52.
3. R. El Guerjouma and et al, Non-destructive evaluation of damage and failure of fiber reinforced polymer composites using ultra sonic waves and acoustic emission, Advanced Engineering Materials, 2001, 3: 601–608.
4. T.P. Philippidis and T.T. Assimakopoulou, Using acoustic emission to assess shear strength degradation in FRP composites due to constant and variable amplitude fatigue loading, Compo Sci&Tech, 2008, 68:840–7.
5. S. Yan, Q. Liang, Q. Guo, Z. Zhou and G. Yu, Analysis on acoustic characteristics of opposed multi-burner gasifier, ApplAcoust, 2011, 72:43–7.
6. A. Albarbar, F. Gu, A.D. Ball and A. Starr, Acoustic monitoring of engine fuel injection based on adaptive filtering techniques, ApplAcoust, 2010, 71:1132–41.
7. A.A. BakhtiaryDavijani, M. Hajikhani and M. Ahmadi, Acoustic Emission based on sentry function to monitor the initiation of delamination in composite materials, Materials and Design, 2011, 32: 3059–3065.
8. N. Godin, S. Huguet, R. Gaertner and L. Salmon, Clustering of acoustic emission signals collected during tensile tests on unidirectionnal glass/polyester composites using supervised and unsupervised classifiers, NDT&E International, 2004, 37 253–264.

9. V. Kostopoulos, T.H. Loutas , A. Kontsos, G. Sotiriadis and Y.Z. Pappas, On the identification of the failure mechanisms in oxide/oxide composites using acoustic emission, NDT&E International, 2003, 36: 571–580.
10. M. Johnson, Waveform based clustering and classification of AE transients in composite laminates using principal component analysis, NDT&E International, 2002, 35: 367–376.
11. N. Godin, S. Huguet and R.Gaertner, Integration of the Kohonen's self-organising map and K-means algorithm for the segmentation of the AE data collected during tensile tests on cross-ply composites, NDT&E International, 2005, 38: 299–309
12. C. Ramirez-Jimenez, N. Papadakis and N. Reynolds, Identification of failure modes in glass/polypropylene composites by means of the primary frequency content of the acoustic emission events, Composites Science and Technology, 2004, 64: 1819–1827.
13. M. Giordano, A. Calabro, C. Esposito, A.D. Amore and L. Nicolais, An acoustic-emission characterization of the failure modes in polymer-composite materials, Composites Science and Technology, 1998, 58 1923–1928.
14. P.J. De Groot, P.A.M. Wijnen and R.B.F. Janssen, Real time frequency determination of acoustic emission for different fracture mechanisms in carbon/epoxy composites, Composites Science and Technology, 1995, 55, 405–412.
15. G. Qi, A. Barhorst, J. Hashemi and G. Kamala, Discrete wavelet decomposition of acoustic emission signals from carbon-fiber reinforced composites, Composites Science and Technology, 1997, 57:389–403.
16. Q-Q. Ni and M. Iwamoto, Wavelet transform of acoustic emission signals in failure of model composites, Engineering Fracture Mechanic, 2002, 69, 717–728.
17. Z. Peng, P. Tse and F. Chua, An improved Hilbert–Huang transform and its application in vibration signal analysis, J Sound Vib, 2005, 286:187–205.
18. E. Hamdi, A. Le Duff, S. Laurent, G. Plantier, A. Sourice and M. Feuilloy, Acoustic emission pattern recognition approach based on Hilbert–Huang transform for structural health monitoring in polymer-composite materials, Applied Acoustics, 2013, 74: 746–757.
19. F.W. King, Hilbert Transforms, Vol. 1, Cambridge University Press, Cambridge, UK, 2009.
20. K. Nie, A. Barco and G. Zeng, Spectral and temporal cues in cochlear implant speech perception, Ear Hear, 2006, 27: 208–217.
21. A. V. Oppenheim and R.W. Schafer, Discrete-Time Signal Processing, 3rd Edition, Pearson, Boston, 2010.
22. A. Recio-Spinoso, Y.-H. Fan and M. Ruggero, Basilar-membrane responses to broadband noise modeled using linear filters with rational transfer functions, Biomedical Engineering, IEEE Transactions, 2011, 58(5): 1456 –1465.
23. M. L. Benzeggagh and M. Kenane, measurement of mixed-mode delamination fracture toughness of unidirectional glass/epoxy composites with mixes- mode bending apparatus, Composites Science and Technology, 1996, 56: 439-449.
24. J. Yousefi, M. Ahmadi, M. Nazmdar, A. Refahi and F. Moghadas, Damage Categorization of Glass/Epoxy Composite Material under Mode II Delamination Using Acoustic Emission Data: A Clustering Approach to Elucidate Wavelet Transformation Analysis, Arab. J. Sci. Eng., 2013, pp. 1-11.
25. M. Fotouhi and M. Ahmadi, Acoustic emission-based study to characterize the initiation of delamination in composite materials, J. Thermoplast. Compos. Mater., DOI: 10.1177/0892705713519811, published online 21 January 2014.
26. P. Compston, P.-Y.B. Jar, P.J. Burchill and K. Takahashi, The effect of matrix toughness and loading rate on the mode-II interlaminar fracture toughness of glass-fibre/vinyl-ester composites, Composites Science and Technology, 2001, 61: 321-333.
27. M. Miura, Ya. Shindo, T. Takeda and F. Narita, Interlaminar fracture characterization of woven glass/epoxy composites under mixed-mode II/III loading conditions at cryogenic temperatures, Engineering Fracture Mechanics, 2012, 96: 615–625.

28. T. Kusaka, K. Watanabe, M. Hojo, T. Fukuoka and M. Ishibashi, Fracture behavior and toughening mechanism in Zanchor reinforced composites under mode II loading, Composites Science and Technology, 2009, 69 2323–2330.
29. J. Bohse, Acoustic emission characteristics of micro failure processes in polymer blends and composites, Composites Science and Technology, 2000, 60: 1213–1226.
30. C. R. Ramirez-Jimenez, N. Papadakis, N. Reynolds, T. H Gan, P. Purnell and M. Pharaoh, Identification of failure modes in glass/polypropylene composites by means of the primary frequency content of the acoustic emission event, Composites Science and Technology, 2004, 64: 1819–1827.
31. W. Haselbach and B. Lauke, Acoustic emission of debonding between fibre and matrix to evaluate local adhesion, Composites Science and Technology, 2003, 63: 2155–2162.
32. Q.Q. Ni and M. Iwamoto, Wavelet transform of acoustic emission signals in failure of model composites, Engineering Fracture Mechanic, 2002, 69: 717–728.

Table 1 Number of specimens with their stacking sequences

Specimen	Mid-plane	Stacking Sequence	Number of Layers
S1	0-0	$[0]_{16}$	16
S2	0-90	$[0,90]_{8s}$	16

Table 2 Dominant Frequency (kHz) range of pure failures

Failure mode	Dominant Frequency (kHz)
Matrix Cracking	140-250
Debonding	250-350

Fiber breakage	350-450

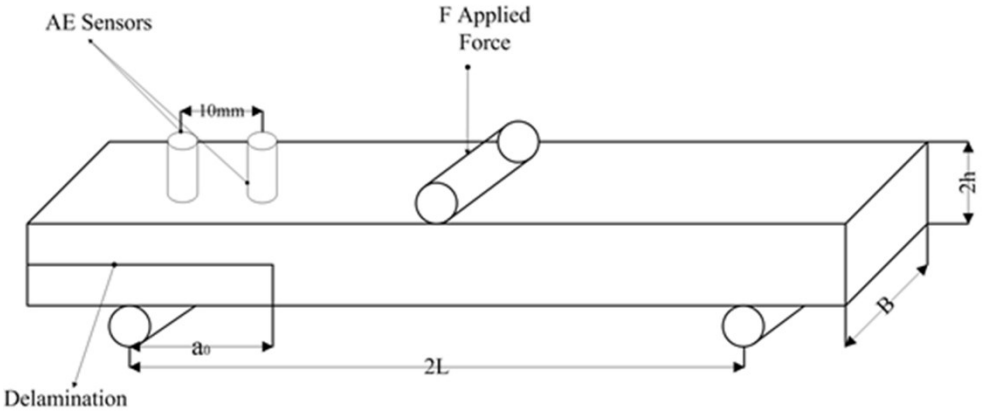

a) Schematically

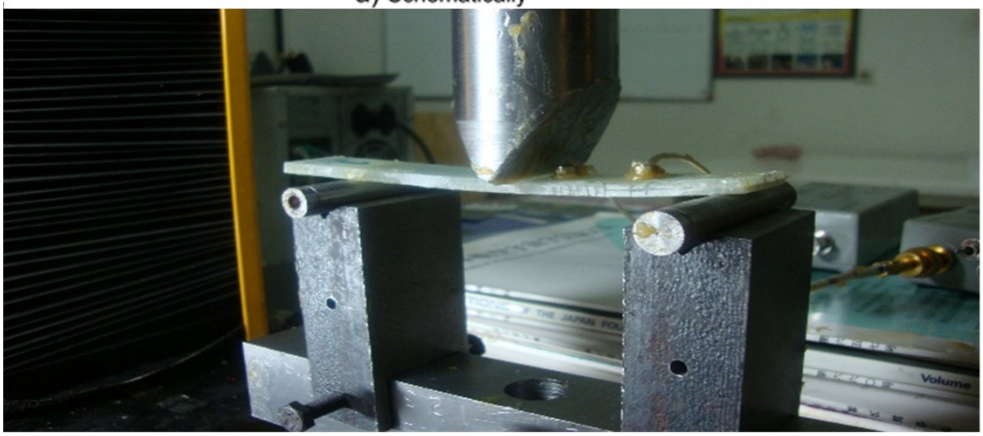

b) physical set-up

Fig. 1 The specimen for three points bending test, End Notch Flexure (ENF)

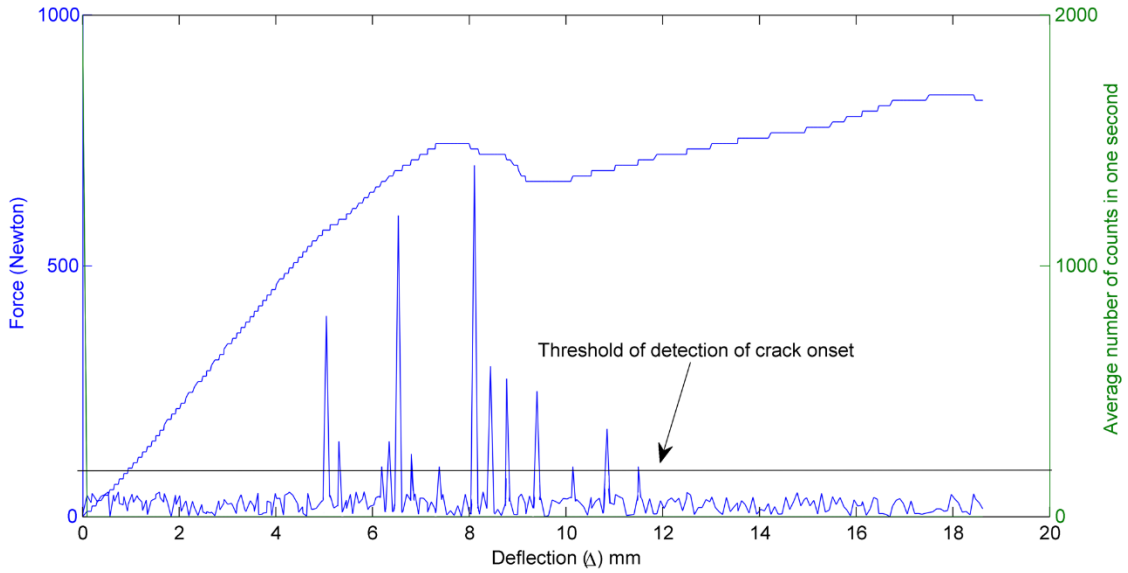

Fig. 2 Force and average number of counts vs. deflection diagram

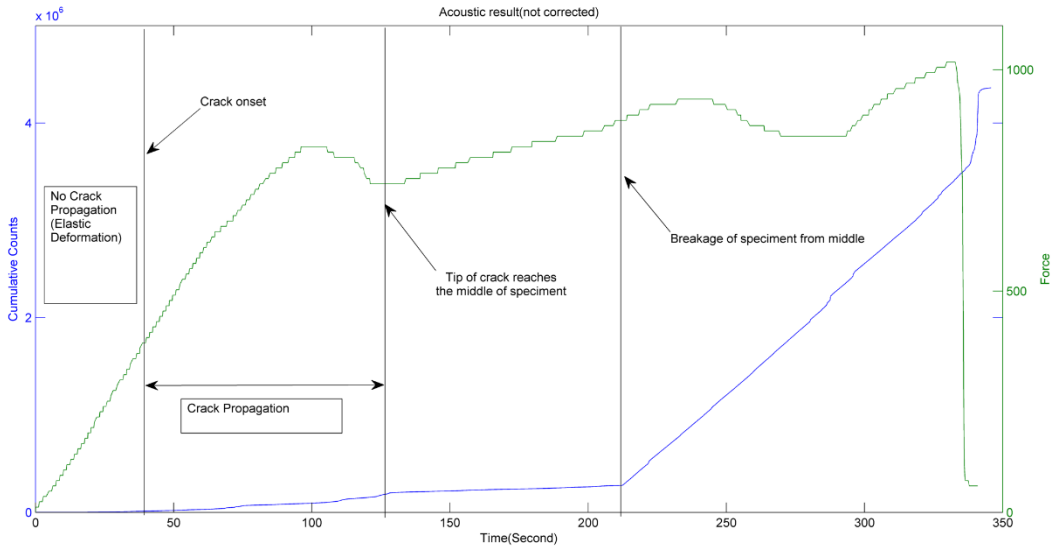

Fig. 3 Cumulative counts of AE events and force (KN) vs. time (second)

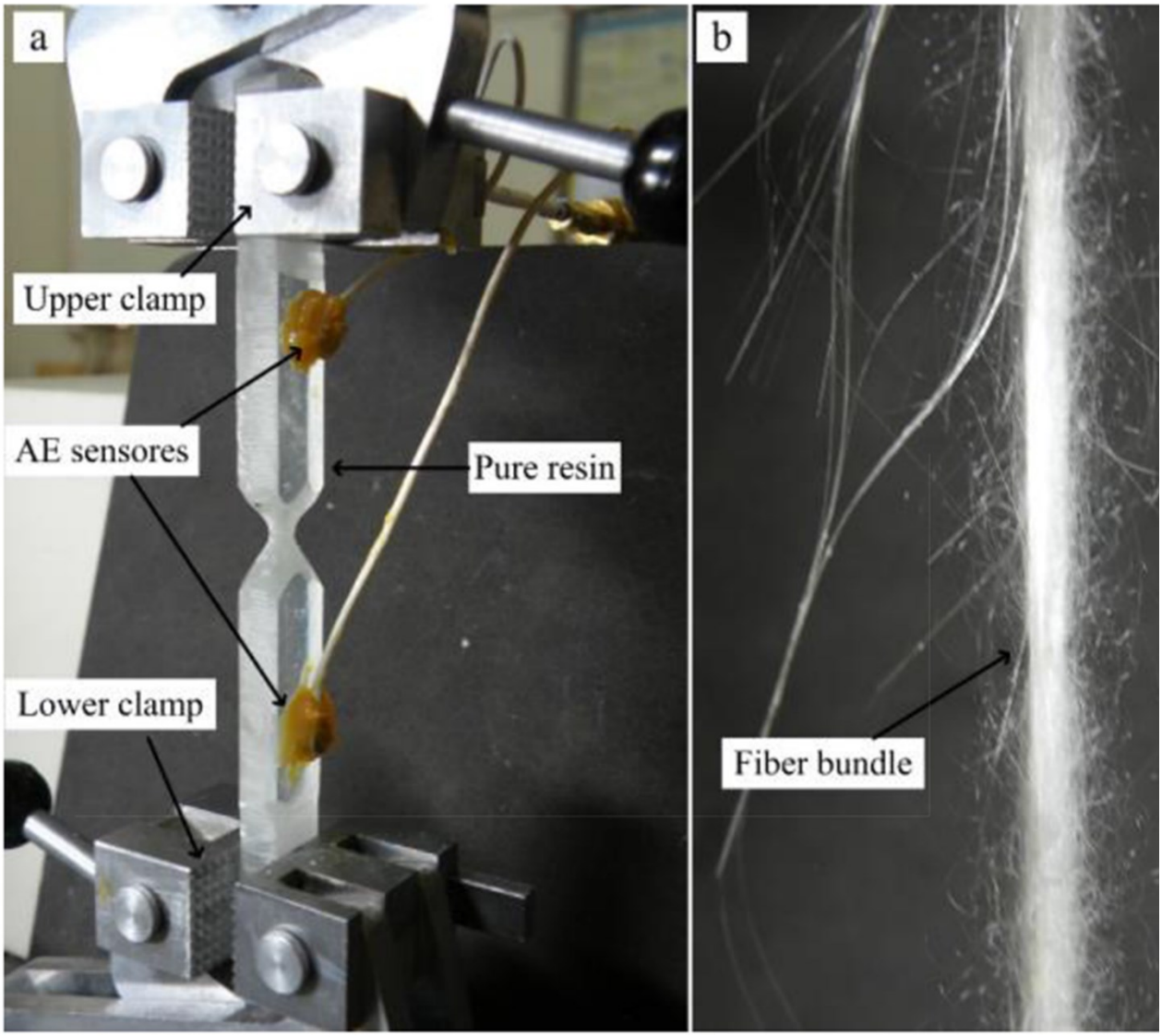

Fig. 4 Experimental procedure of pure matrix cracking and fiber breakage

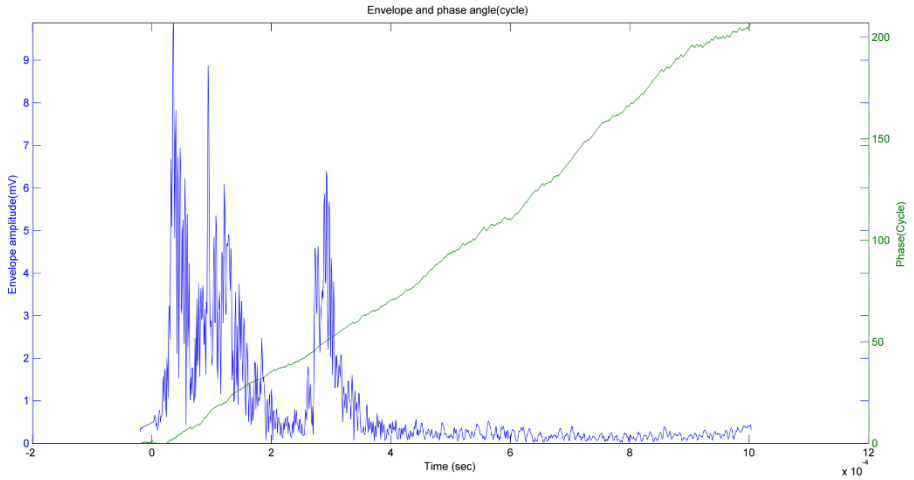

Fig. 5 Phase angle and Hilbert transform of pure matrix cracking

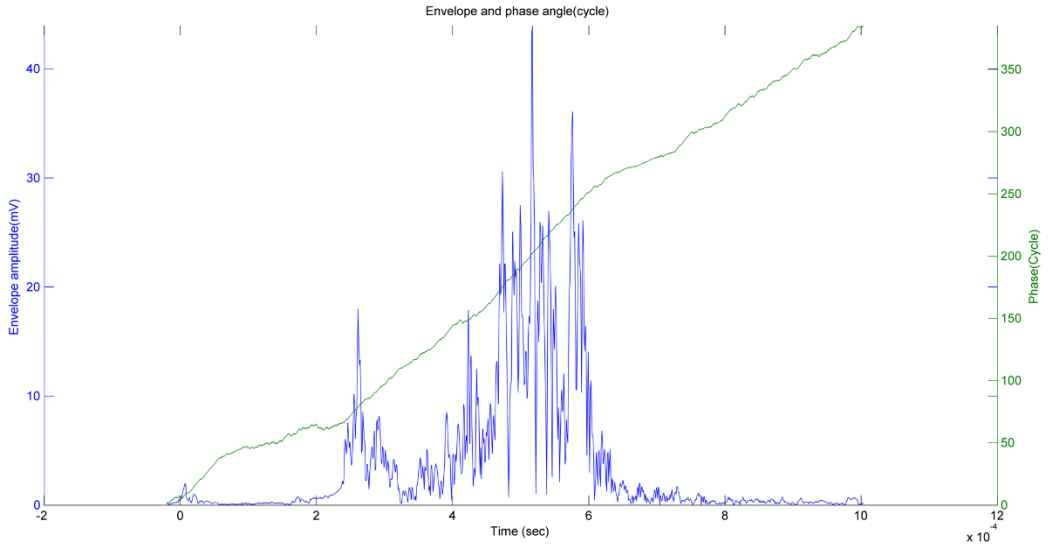

Fig. 6 Phase angle and Hilbert transform of pure fiber breakage

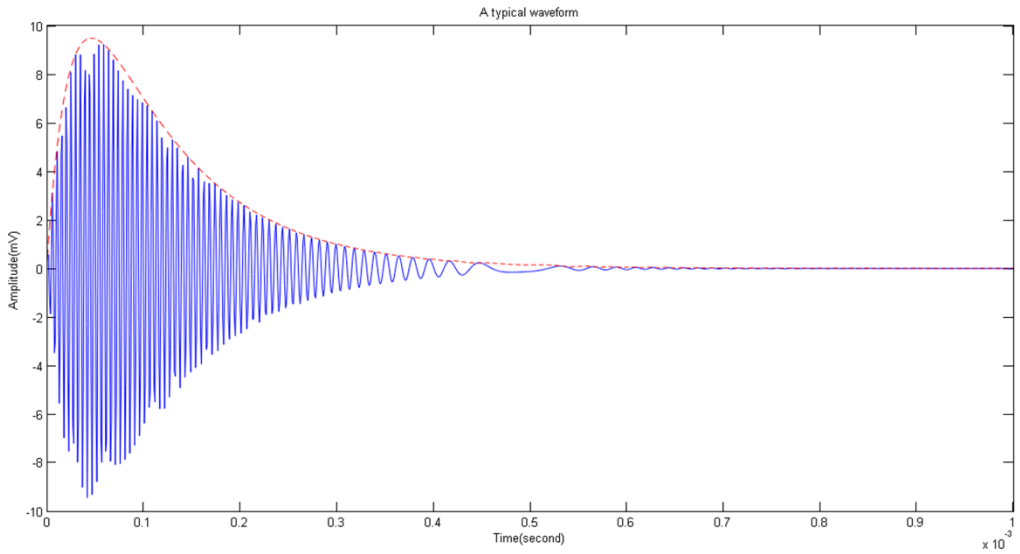

Fig. 7 A typical sample of acoustic wave with its Envelope trend

.

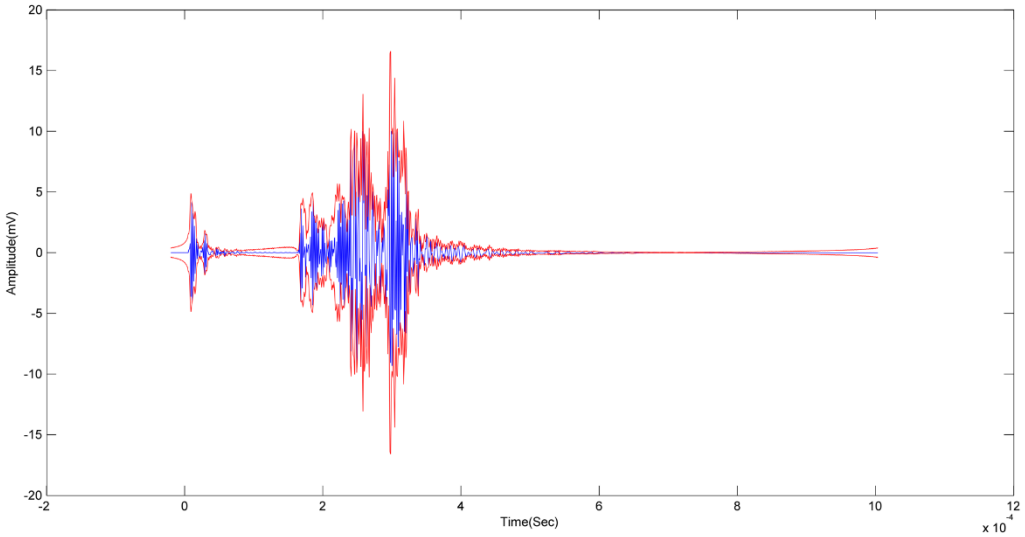

Fig. 8 A sample AE wave in three points bending test with its envelope (time(S) vs. amplitude (mV))

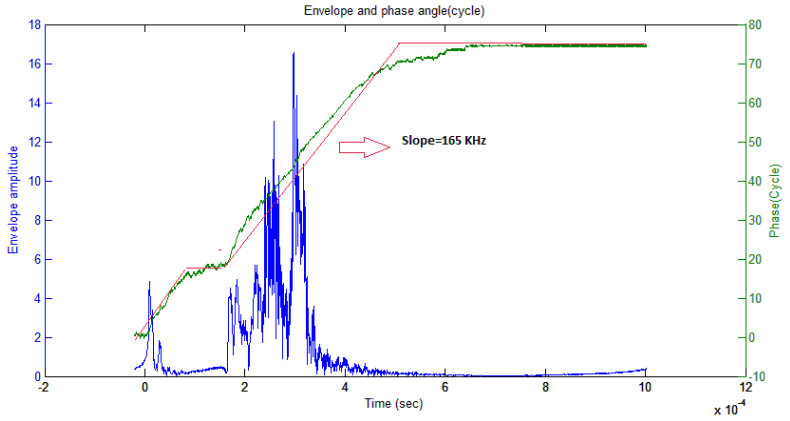

Fig. 9 approximation of envelope and phase angle vs. time(s)

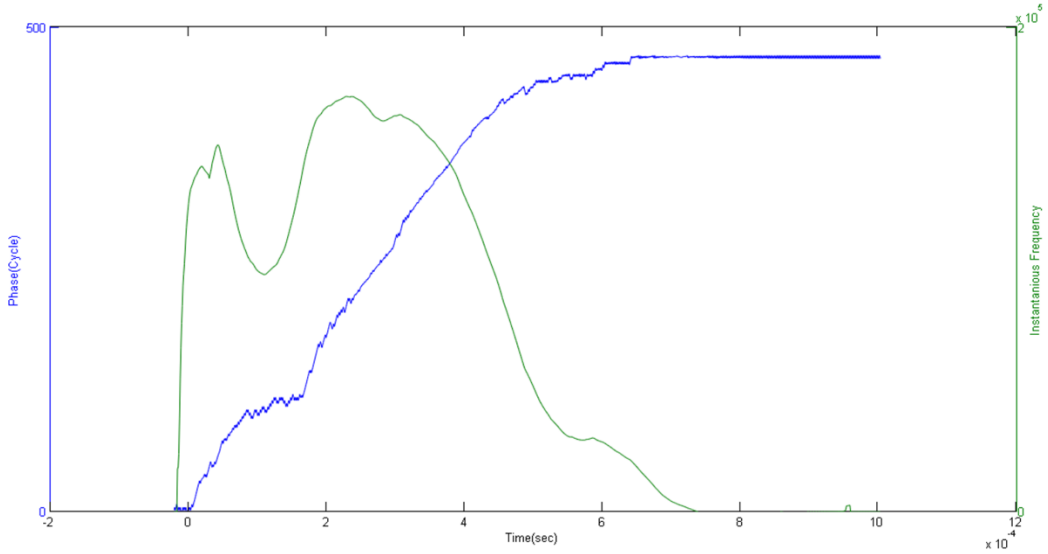

Fig. 10 instantaneous frequency and phase angle vs. time

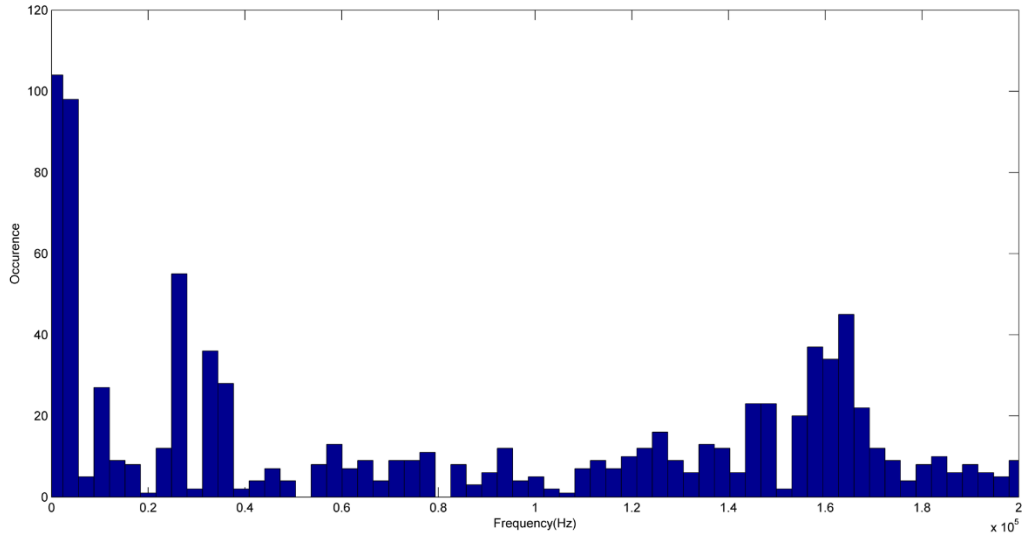

Fig. 11 distribution of instantaneous frequency in 2 KHz frequency intervals

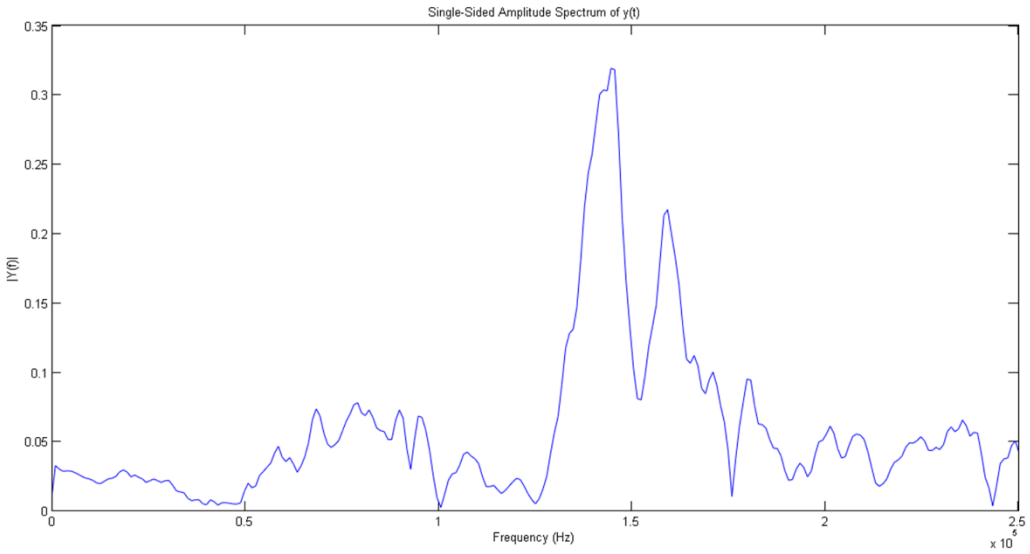

Fig. 12 Fourier transform of the main wave

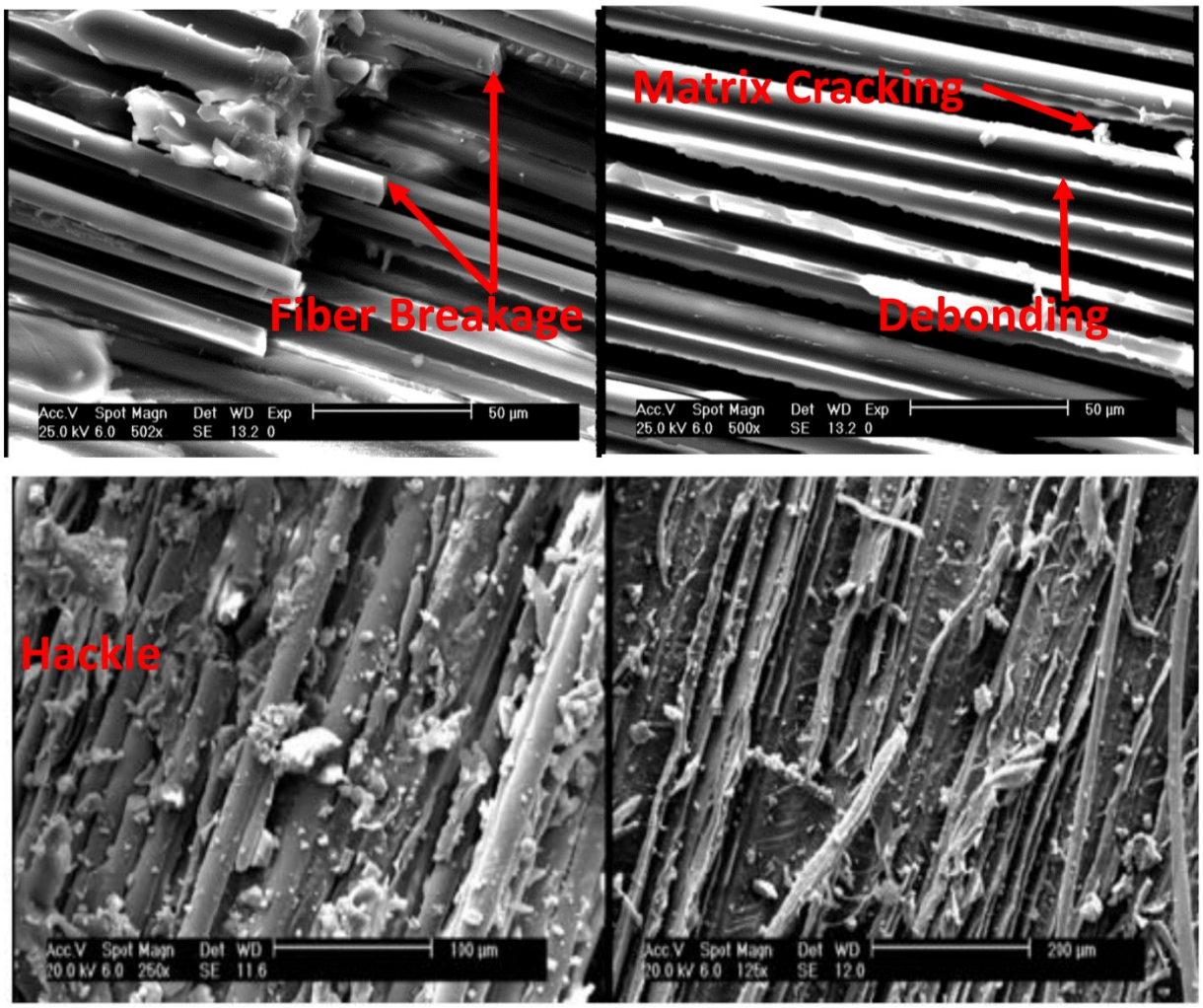

Fig. 13 SEM observation of different failure mechanisms during mode II delamination

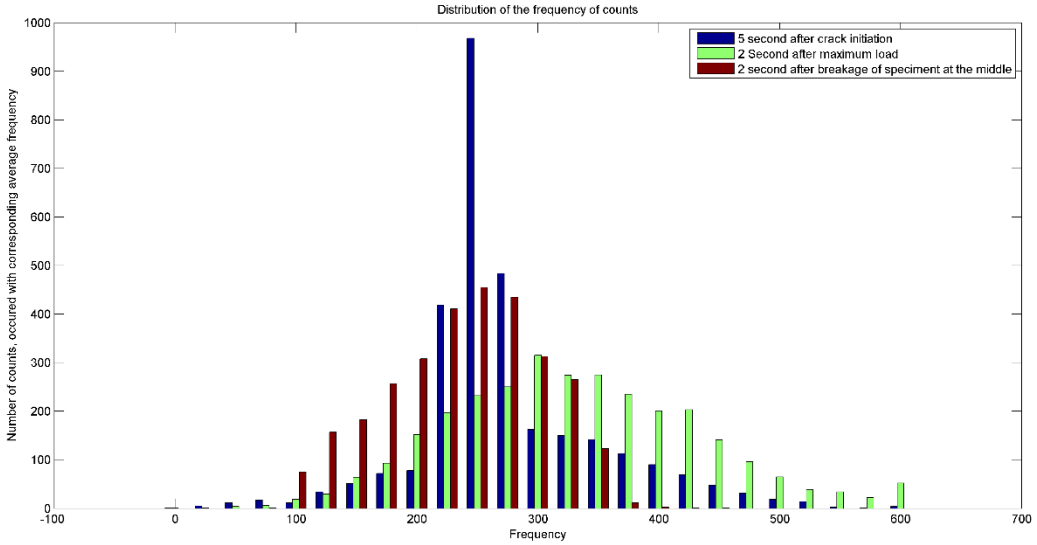

Fig. 14 Distribution of frequency of counts among all AE waveforms for a sample specimen